




# The study of external growth environments on the crystal morphology of $\epsilon$ -HNIW by molecular dynamics simulation

Guanchao Lan<sup>1</sup>, Shaohua Jin<sup>1</sup>, Jing Li<sup>1</sup>, Junying Wang<sup>1</sup>, Jinxin Li<sup>2</sup>, Shusen Chen<sup>1</sup>, and Lijie Li<sup>1,\*</sup> 

<sup>1</sup>School of Materials Science and Engineering, Beijing Institute of Technology, Beijing 100081, China

<sup>2</sup>Gansu Yin Guang Chemical Industry Group Co. Ltd, Baiyin 730900, China

Received: 21 December 2017

Accepted: 4 June 2018

Published online:

11 June 2018

© Springer Science+Business Media, LLC, part of Springer Nature 2018

## ABSTRACT

Attachment energy model was adopted to research the influence of external growth environments on  $\epsilon$ -HNIW crystal morphology. The morphology of  $\epsilon$ -HNIW crystal in acetone–cyclohexane binary systems was simulated with cyclohexane mass fraction of 0.05, 0.10, 0.15 and 0.20, respectively. The influences of 0.80 acetone on  $\epsilon$ -HNIW morphology were studied in the acetone–toluene, acetone–benzene and acetone–dichloromethane binary system. Besides, the effects of the temperature and supersaturation on  $\epsilon$ -HNIW crystal morphology were also examined in the acetone–cyclohexane system. The simulation results reveal that  $\epsilon$ -HNIW crystal morphology almost maintains consistent with the increase in cyclohexane ratio. Contrarily, the variations of the anti-solvent, the temperature and the supersaturation affect  $\epsilon$ -HNIW crystal morphology dramatically. Furthermore, the influence of model dimension on the attachment energy was discussed, and a reasonable model size was obtained. The radial distribution function analysis was performed to explore the adsorption and diffusion behaviours of the solvent molecules on the  $\epsilon$ -HNIW surfaces. Overall, the simulation results can provide some guidance for the crystallization process of  $\epsilon$ -HNIW.

## Introduction

As the representative of high energy density materials (HEDMs), hexanitrohexaazaisowurtzitane (HNIW) has attracted much attention since it was first synthesized by Nielsen [1]. Compared with octahydro-1,3,5,7-tetranitro-1,3,5,7-tetrazocine (HMX), HNIW possesses higher energy, greater density,

stronger detonation pressure, faster detonation velocity as well as higher sensitivity [2, 3]. Sensitivity is a critical property of energetic material that is directly affected by the crystal morphology. Crystals with needle- or plate-like morphology exhibit higher impact and friction sensitivity than that with sphere-shaped crystals of the same size [4]. That is to say, energetic materials can be desensitized by modifying

Address correspondence to E-mail: lilijie2003@bit.edu.cn

the crystal morphology. Accordingly, it is of important value to investigate the technique of morphology control for the application of HNIW.

The irregular crystal morphology of the energetic materials hinders its application. The morphology is determined by both the internal structure factors and the external conditions [5]. Crystallization is a traditional way to control the morphology by changing solvents, additives and adjusting operation conditions, among which the solvent is considered to be one of the most important factors [6–8]. By combining experiment and computation, the influence of solvent on crystal morphology from macroeconomic and microeconomic can be investigated. Computational simulation can achieve the goal in an economical and environment-friendly way, with more microscopic details of the interaction between solvent and crystal. Experiment can examine the accuracy of the simulation. The development of computational technology has generated many simulation methods for the prediction of the crystal morphology, and molecular dynamics (MD) simulation that can provide atomic-scale information has become a powerful one of these methods [5]. Numerous researches have successfully simulated the crystal morphology by MD method [9–16].

In this study, acetone was selected as the solvent for HNIW, while cyclohexane, toluene, benzene and dichloromethane were selected as the anti-solvents [17]. In order to build a crystal/solvent double-layered model with reasonable size for the molecular dynamic simulations, we have discussed the influences of supercell crystal length, width, thickness and the amount of solvent on the attachment energy in the paper. On this basis, Materials Studio (MS) 6.0 software was employed to predict the morphology of HNIW crystals in acetone–cyclohexane binary systems with the cyclohexane mass fraction of 0.05, 0.10, 0.15 and 0.20, as well as that in acetone–toluene, acetone–benzene and acetone–dichloromethane binary system with acetone mass fraction of 0.80. Furthermore, the influence of the temperature ranging from 298 to 328 K together with the supersaturation ranging from 1.00 to 1.35 on the morphology was investigated systematically.

Currently, many researchers adopt attachment energy (AE) model to study the influence of solvent or additive on the crystal morphology [18, 19]. In addition, most articles extend a single-crystal surface to a  $3 \times 3 \times 3$  supercell to calculate the solvent-effect

attachment energy [10, 14, 18, 20–23]. But  $3 \times 3 \times 3$  supercell is not an universal size, and for many crystal surfaces the accuracy of this size is low. Besides, there is no unified standard for adding how many solvent molecules, which is an important parameter for the morphology simulation. In this study, we systematically investigated the influences of supercell crystal length, width, thickness and the amount of solvent on the attachment energy. Based on the results, we proposed a reasonable size of solvent/crystal surface double-layered model. The size can be applied to other crystal morphology study. Eventually, we predicted the morphology of HNIW in different binary systems, when the model size was confirmed.

## Computational and experimental

### Theory

The morphology of crystals can be affected by many factors such as temperature, solubility, supersaturation, additive, solvent and adsorption energy of solvent and solute molecules [22]. The classic attachment energy (AE) model assumes that the relative growth rate of a crystal surface is proportional to the absolute value of the attachment energy of the corresponding crystal surface [26]. Most crystals are grown from solvent which can reduce the growth rate of crystal surfaces, because the solvent molecules have to be removed from the surface before the crystal face growth. This costs energy and herewith the attachment energy decreases. Therefore, the classic AE model is failure to simulate crystals morphology grown from solution, which may be attributed to disregarding the external crystallization conditions. Since the effects of the growth environment have been taken into account, the classic attachment energy (AE) model that neglects the external crystallization conditions should be modified accordingly [21].

Based on two-dimensional nucleation mechanism [24], the growth rate of crystal surface is mostly dominated by the nucleation rate of the surface ( $J$ ). Then, the normal growth rate of crystal face ( $R_{hkl}$ ) can be expressed by the following equation:

$$R_{hkl} = hSJ \quad (1)$$

where  $h$  is the height of the step formed by nucleation, generally thought as the interplanar space [25],

and  $S$  stands for the area of the surface swept by the two-dimensional critical nucleus. The nucleation rate of the crystal surface is expressed as:

$$J = v_0 \exp\left(-\frac{\Delta G_C}{kT}\right) \tag{2}$$

where  $v_0$  is the collision frequency of atoms or molecules in the growth surface,  $\Delta G_C$  represents the system Gibbs energy change when the formation of a stable critical size of crystal nucleus in the growth surface. The  $\Delta G_C$  can be calculated by the following equation [26, 27]

$$\Delta G_C = \frac{\pi h \gamma \omega}{kT\sigma} \tag{3}$$

where  $\gamma$  is the surface free energy in solution,  $\omega$  stands for the molecular specific volume and  $kT\sigma$  represents the driving force of solution growth.

Hartman [26] has proposed the following equation to show the relation between the attachment energy ( $E_{att}$ ) of the crystal face and its surface free energy

$$\gamma_{hkl} \cong -\frac{ZE_{att}d_{hkl}}{N_A V_p} \tag{4}$$

where  $Z$  is the number of molecules of formula units in a primitive unit cell of volume,  $d_{hkl}$  represents the interplanar spacing of the lattice, and  $V$  stands for mesh area.

Saska [28] has concluded that the change of crystal surface free energy in solution resulted from the adsorption interactions between solvents and crystal faces, which can be calculated by the following formula,

$$\Delta\gamma = \frac{ZE_S d_{hkl}}{N_A V_p} \tag{5}$$

where  $E_S$  represents the solvent adsorption interactions. Therefore,  $\gamma$  in solution can be rewritten as:

$$\gamma = \gamma_{hkl} - \Delta\gamma = -\frac{Z(E_{att} - E_S)d_{hkl}}{N_A V_p} \tag{6}$$

Combining Eqs. (3) and (6), the following equation can be derived as:

$$\Delta G_C = \frac{\pi h \omega Z d_{hkl}}{kT\sigma N_A V_p} (E_{att} - E_S) \tag{7}$$

Then, a deformation of Eq. (1) can be obtained as:

$$R_{hkl} = hSv_0 \exp\left[-\frac{\pi h \omega Z d_{hkl}}{k^2 T^2 \sigma N_A V_p} (E_{att} - E_S)\right] \tag{8}$$

where  $Z$ ,  $d_{hkl}$  and  $V_p$  are crystal bulk properties. For a

given solution crystallization condition such as the determined  $T$  and  $\sigma$ , when the two-dimensional nucleation growth mechanism is obeyed, it is seen from Eq. (8) that  $R_{hkl}$  is shown to be approximately proportional to the  $(E_{att} - E_S)$

$$R_{hkl} \propto (E_{att} - E_S) \tag{9}$$

The modified attachment energy ( $E_{att}^S$ ) is defined to represent the  $(E_{att} - E_S)$ . And  $E_S$  can be calculated by the following equation,

$$E_S = E_{int} \times \frac{A_{acc}}{A_{box}} \tag{10}$$

where  $A_{acc}$  is the solvent-accessible area of the crystal face in the unit cell,  $A_{box}$  is the super crystal face area of the  $(h k l)$  plane, and  $E_{int}$  is the interaction energy between the solvent and crystal surface that can be calculated by the following equation,

$$E_{int} = E_{tot} - E_{surf} - E_{solv} \tag{11}$$

where  $E_{tot}$  stands for the total energy of the solvent layer and crystal surface,  $E_{surf}$  represents the energy of the crystal surface without the solvent layer, and  $E_{solv}$  is the energy of the solvent layer without the crystal surface.

### Simulation details

At ambient temperature and 0.1 MPa, HNIW exists in four different polymorphic modifications, i.e.  $\alpha$ ,  $\beta$ ,  $\gamma$  and  $\epsilon$ , among which  $\epsilon$ -HNIW with lattice parameters of  $a = 13.696 \text{ \AA}$ ,  $b = 12.554 \text{ \AA}$ ,  $c = 8.833 \text{ \AA}$ ,  $\beta = 111.18^\circ$  [29] possesses the highest stability and has higher value in application compared with other polymorphs. Therefore,  $\epsilon$ -HNIW was used to conduct the MD simulations in this study. The geometry of the unit lattice is optimized through smart algorithm of Forcite module under COMPASS force field which has been parameterized and validated by the prediction of condensed phase properties [5]. The experimental lattice parameters and the optimized values of  $\epsilon$ -HNIW are listed in Table 1. It can be found that the relative deviations between the optimized lattice parameters and the experimental values are within 2%, which demonstrates that the COMPASS force field is suitable for the simulation of  $\epsilon$ -HNIW.

The vacuum morphology of  $\epsilon$ -HNIW was predicted by the AE model. The dominant faces exposed on  $\epsilon$ -HNIW crystal in vacuum were built by cleaving

**Table 1** Comparison of the experimental and optimized lattice parameters of  $\epsilon$ -HNIW

Lattice parameter	$a$ (Å)	$b$ (Å)	$c$ (Å)	$\beta$ (°)
Experiment	13.696	12.254	8.833	111.180
COMPASS	13.729	12.258	8.731	112.464
Relative error (%)	0.241	0.033	− 1.155	1.155

the surface along the corresponding ( $h k l$ ) directions. Then, the solvent amorphous cells were built, of which the lengths and widths should match the sizes of  $\epsilon$ -HNIW faces and the thicknesses depended on the amount of the solvent molecules.

The dynamic simulation of 400 ps for each face was performed in NVT ensemble under COMPASS force field at the given temperature with the Andersen thermostat. The electrostatic interaction was calculated by Ewald method with an accuracy of  $0.0001 \text{ kcal mol}^{-1}$ , and van der Waals force was computed by the atom-based method with the cut-off distance of  $15.5 \text{ \AA}$ .

## Experimental process

The incubator was used to cultivate  $\epsilon$ -HNIW crystals in acetone–cyclohexane binary systems with the cyclohexane mass fraction of 0.05, 0.10, 0.15 and 0.20, as well as that in acetone–toluene, acetone–benzene and acetone–dichloromethane binary system with acetone mass fraction of 0.80 under 298 K. Similarly,  $\epsilon$ -HNIW crystals were cultivated in the acetone–cyclohexane binary system at 298, 308, 318 and 328 K, respectively. Then, the morphology of the recrystallization samples of  $\epsilon$ -HNIW was observed using scanning electron microscopy (SEM) to test the consistency between the computational results and experimental results.

## Results and discussion

### Vacuum morphology of $\epsilon$ -HNIW

The crystal morphology of  $\epsilon$ -HNIW in vacuum with six dominant faces calculated by the AE model is exhibited in Fig. 1a. The predicted crystal habit under vacuum conditions is similar to the spherical shape with an aspect ratio of 1.436. The molecular interactions between  $\epsilon$ -HNIW molecules calculated by

morphology module and visualized by crystal graph are shown in Fig. 1b. It has been proven that the growth rate of crystal increases as the interaction becomes stronger [30]. In Fig. 1b, the blue lines represent strong interactions, while the red lines represent weak interactions, which means that  $\epsilon$ -HNIW grows faster along the direction of blue lines than that of red lines. On the basis of the periodic bond chain (PBC) theory, the strongest bonds usually exist in the direction along which crystals grow fastest. The faces with fast growth rates will disappear and the surfaces with slow growth rates will occupy the final crystal surface, resulting in the crystal habit of  $\epsilon$ -HNIW in vacuum dominated by six faces. The relevant parameters of the six dominant faces (1 1 0) (1 1 − 1) (0 0 1) (2 0 0) (0 1 1) and (2 0 − 1) are listed in Table 2. Among them, the (1 1 0) face, with the largest total habit facet area percentage  $S\%$ , possesses the strongest morphological importance.

In order to understand the interactions between solvent molecules and different  $\epsilon$ -HNIW crystal faces, the molecular packing structures of  $\epsilon$ -HNIW crystal faces are displayed in Fig. 2, in which the blue grid on the  $\epsilon$ -HNIW crystal face stands for the accessible solvent surface. The calculated solvent-accessible area ( $A_{\text{acc}}$ ), surface area ( $A_{hkl}$ ) and corresponding  $A_{\text{acc}}/A_{hkl}$  values for different crystal faces of  $\epsilon$ -HNIW are presented in Table 3. From the molecular arrangement of  $\epsilon$ -HNIW morphologically significant surfaces, it is illustrated that the (2 0 0) (1 1 − 1) (2 0 − 1) and (1 1 0) faces are relatively flat at molecular level, while (0 1 1) and (0 0 1) are uneven with many large voids. Accordingly, a larger value of  $A_{\text{acc}}/A_{hkl}$  indicates a more complex surface topography easy for the adsorption of solvent molecules, probably resulting in a larger energy correction term  $E_s$  and dramatically influencing the final morphology. Besides, the exposed atoms of different  $\epsilon$ -HNIW crystal faces are different as well, which may have a great effect on the interaction between  $\epsilon$ -HNIW faces and solvent.

### The influence of model size on $E_{\text{att}}^S$

Model dimension is a key factor that influences the  $E_{\text{att}}^S$  and thus significantly affects the final predicted morphology. If the model dimension is too small, the deviation of the calculated  $E_{\text{att}}^S$  will be large, which results in inaccurate simulated results. On the contrary, if the model size is too large, the simulation will

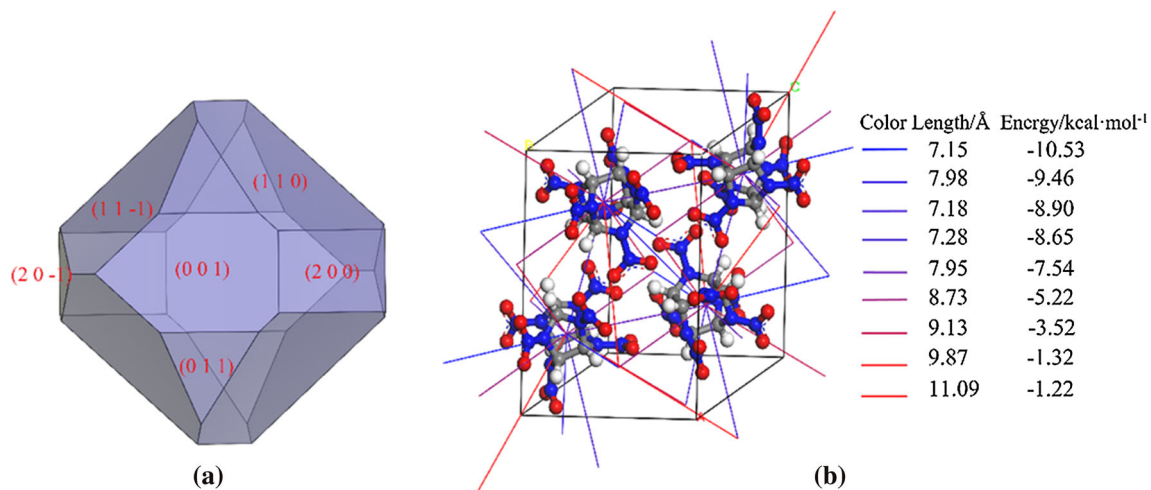


**Figure 1** a Crystal morphology and b molecular interactions of ε-HNIW in vacuum calculated by AE model.

**Table 2** Parameters of the dominant crystal faces of ε-HNIW

$(h\ k\ l)$	Multiplicity	$d_{hkl}$ (Å)	$A_{hkl}$ (Å <sup>2</sup> )	$E_{att}$ (Total) (kcal mol <sup>-1</sup> )	S%
(1 1 0)	4	8.82	154.03	- 86.71	39.55
(1 1 - 1)	4	6.94	195.67	- 92.97	26.06
(0 0 1)	2	8.07	168.30	- 89.71	13.16
(2 0 0)	2	6.34	107.03	- 94.90	10.26
(0 1 1)	4	6.74	201.49	- 97.94	8.17
(2 0 - 1)	2	6.29	215.90	- 112.30	2.79

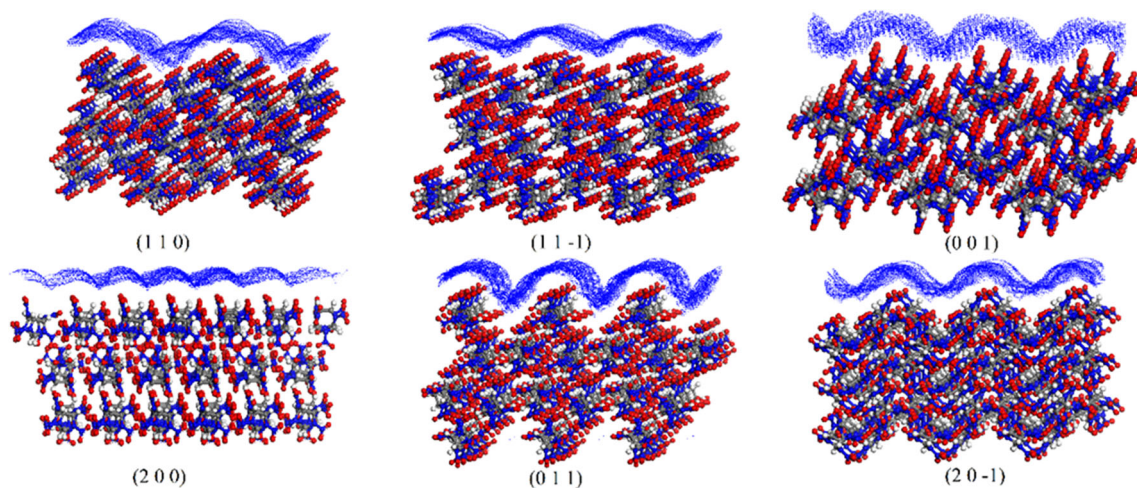


**Figure 2** Geometric structures of different ε-HNIW crystal faces with the blue grid denoting the accessible solvent surface.

**Table 3** Parameters for the crystal surfaces of ε-HNIW

	(1 1 0)	(1 1 - 1)	(0 0 1)	(2 0 0)	(0 1 1)	(2 0 - 1)
$A_{acc}/\text{Å}^2$	245.53	267.02	292.18	137.33	396.82	325.14
$A_{hkl}/\text{Å}^2$	154.03	195.67	168.30	107.03	201.49	215.90
$A_{box}/\text{Å}^2$	1232.27	1761.01	1514.71	1284.34	1813.37	1295.42
$A_{acc}/A_{hkl}$	1.59	1.36	1.74	1.28	1.97	1.51

last a long time without a considerable promotion of the accuracy. Therefore, it is a critical step to find out a suitable model size to meet the accuracy requirement and consume less time. In this study, the influence of model size on the  $E_{\text{att}}^{\text{S}}$  was systematically investigated as follows. Firstly, the size of solvent amorphous cell is fixed, and the thickness of HNIW crystal surface ( $t_c$ ) is changed to search the suitable  $t_c$ . Secondly, the size of HNIW supercell is fixed, and the thickness of the solvent ( $t_s$ ) is changed to select the suitable  $t_s$ . Thirdly, the  $t_c$  and  $t_s$  are fixed, and the area of HNIW surface is changed to search the suitable area. The detailed steps are displayed in Fig. 3.

The (1 1 0) with the largest  $S\%$  and (0 1 1) with the largest  $A_{\text{acc}}/A_{\text{hkl}}$  were taken as examples to illustrate the influence of model size on  $E_{\text{att}}^{\text{S}}$ . The calculated  $E_{\text{att}}^{\text{S}}$  affected by the model size is summarized in Table 4 and Fig. 4.

The simulation results demonstrate that with the increase in the model size, the  $E_{\text{att}}^{\text{S}}$  increases rapidly initially and then almost maintains constant. The studies of the influences of the solvent thickness ( $t_s$ ) and crystal thickness ( $t_c$ ) on the  $E_{\text{att}}^{\text{S}}$  reveal that when  $t_s$  and  $t_c$  are smaller than the cut-off distance ( $d_c$ ) of van der Waals forces, the  $E_{\text{att}}^{\text{S}}$  increases rapidly, and when  $t_s$  and  $t_c$  are larger than  $d_c$ , the  $E_{\text{att}}^{\text{S}}$  almost maintains constant. Thus, the  $t_s$  and  $t_c$  of the model should be no less than  $d_c$ , or the accuracy will be low, and it is unnecessary to set the  $t_s$  and  $t_c$  too large. The investigation of the influence of crystal area on the  $E_{\text{att}}^{\text{S}}$  reveals that when both the length and width of the supercell are less than  $2d_c$ , the  $E_{\text{att}}^{\text{S}}$  increases with the increase in the length and width, and when both the length and width are larger than  $2d_c$ , the  $E_{\text{att}}^{\text{S}}$  almost maintains unchanged. Therefore, a

$\epsilon$ -HNIW crystal/solvent model with the length and width of the supercell no less than  $2d_c$  and the  $t_s$  and  $t_c$  larger than  $d_c$  should be constructed to meet the accuracy and simulation time requirement. Since the intermolecular interactions between  $\epsilon$ -HNIW and solvent molecules are mainly hydrogen bonds, van der Waals forces and electrostatic interactions, the effective range of these non-bond energies should be within the  $d_c$ . When the  $t_s$  is much larger than  $d_c$ , the solvent molecules far from the  $\epsilon$ -HNIW supercell have little interaction with  $\epsilon$ -HNIW, so they have little effect on the simulation results, and so is the  $t_c$ . Meanwhile, the length and width of the model should be greater than  $2d_c$ . Taking a solvent molecule as an example, the interaction range between solvent and crystal is within the red circle, as shown in Fig. 5. Therefore, if the width or length is less than  $2d_c$ , the interaction between the solvent and the atoms of  $\epsilon$ -HNIW molecules that beyond the range may be neglected. Besides, if the size of the crystal area is too large, the atoms that beyond the red circle have almost no interaction with the solvent, so both the length and width of  $\epsilon$ -HNIW supercell should be  $2d_c$ .

### The influence of anti-solvent ratio on $\epsilon$ -HNIW morphology

Industrially, most crystals grow from solution, which affects the morphology remarkably. Compared with those in vacuum, crystals of  $\epsilon$ -HNIW grown from solution need to remove solvent molecules adsorbed on the surfaces, which consumes some energy. The consumed energy is the energy correction term  $E_S$ , which can be calculated by the interaction energy between  $\epsilon$ -HNIW surfaces and solvent molecules.

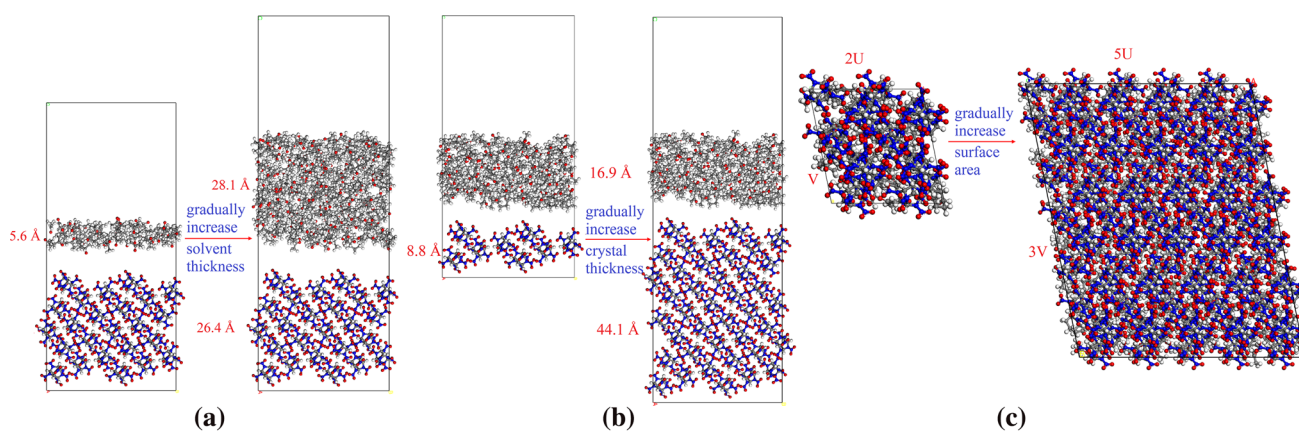


**Figure 3** Investigation procedure of the influence of **a** solvent thickness, **b** crystal thickness, **c** crystal area on  $E_{\text{att}}^{\text{S}}$ .

**Table 4** Influence of solvent thickness ( $t_s$ ), crystal thickness ( $t_c$ ) and crystal area ( $S$ ) on  $E_{att}^S$

	Size/Å	$E_{tot}$ (kcal mol <sup>-1</sup> )	$E_{surf}$ (kcal mol <sup>-1</sup> )	$E_{solv}$ (kcal mol <sup>-1</sup> )	$E_{int}$ (kcal mol <sup>-1</sup> )	$E_{att}^S$ (kcal mol <sup>-1</sup> )
<i>(1 1 0)</i>						
$t_s$	5.63	- 29218.60	- 28260.49	- 619.08	- 339.03	- 19.16
	11.25	- 30074.20	- 28291.92	- 1418.46	- 363.82	- 14.23
	16.88	- 30849.30	- 28287.89	- 2177.46	- 383.94	- 10.21
	22.50	- 31764.03	- 28312.41	- 3070.60	- 381.02	- 10.79
	28.13	- 32553.56	- 28246.00	- 3925.13	- 382.43	- 10.51
$t_c$	8.82	- 10803.47	- 9002.29	- 1445.13	- 356.05	- 15.77
	17.63	- 21282.51	- 18640.64	- 2261.02	- 380.84	- 10.83
	26.45	- 30849.30	- 28287.89	- 2177.46	- 383.94	- 10.21
	35.26	- 40553.62	- 37905.12	- 2264.73	- 383.76	- 10.25
	44.08	- 50320.07	- 47664.74	- 2270.41	- 384.92	- 10.01
$S$	2U × V	- 5309.35	- 4649.73	- 579.19	- 80.42	- 22.62
	2U × 2V	- 10634.45	- 9310.58	- 1149.03	- 174.85	- 17.04
	3U × 2V	- 15873.60	- 13983.19	- 1616.33	- 274.08	- 13.90
	4U × 2V	- 21282.51	- 18640.64	- 2261.02	- 380.84	- 10.83
	4U × 3V	- 31672.63	- 27938.60	- 3164.48	- 569.55	- 11.06
	5U × 3V	- 39558.68	- 34931.20	- 3913.27	- 714.21	- 10.82
<i>(0 1 1)</i>						
$t_s$	5.18	- 32814.58	- 31391.21	- 832.51	- 590.85	31.35
	10.36	- 34014.34	- 31413.48	- 1927.73	- 673.12	49.36
	15.54	- 35167.34	- 31427.61	- 3037.61	- 702.12	55.70
	20.66	- 36279.59	- 31352.15	- 4225.24	- 702.20	55.72
	25.85	- 37391.57	- 31390.94	- 5297.34	- 703.30	55.96
$t_c$	6.84	- 13799.10	- 10044.08	- 3180.15	- 574.87	27.86
	13.67	- 24431.16	- 20631.77	- 3152.22	- 647.17	43.68
	20.51	- 35167.34	- 31427.61	- 3037.61	- 702.12	55.70
	27.34	- 46122.64	- 42261.51	- 3159.11	- 702.01	55.68
	34.18	- 56916.90	- 53066.47	- 3149.62	- 700.81	55.42
	41.02	- 67711.16	- 63911.39	- 3141.13	- 700.81	55.42
$S$	2U × V	- 7897.39	- 7015.43	- 764.57	- 117.39	17.65
	2U × 2V	- 15859.87	- 14103.19	- 1497.98	- 258.70	29.44
	3U × 2V	- 23444.55	- 20948.11	- 2049.29	- 447.16	48.83
	3U × 3V	- 35167.34	- 31427.61	- 3037.61	- 702.12	55.70
	4U × 3V	- 46952.40	- 41891.92	- 4128.70	- 931.78	54.98
	4U × 4V	- 62556.93	- 55858.80	- 5451.43	- 1246.70	55.52

When the  $E_S$  is obtained, the solvent-effected attachment energy  $E_{att}^S$  can be computed, and then, the morphology of  $\epsilon$ -HNIW crystal can be predicted. Generally,  $\epsilon$ -HNIW is mainly obtained by anti-solvent crystallization method. Acetone and cyclohexane are commonly used as solvent and anti-solvent for  $\epsilon$ -HNIW crystallization, respectively. In order to investigate the influence of anti-solvent ratio on  $\epsilon$ -HNIW crystal morphology, the morphology of  $\epsilon$ -HNIW crystals in acetone–cyclohexane binary systems with cyclohexane mass fraction of 0.05, 0.10, 0.15 and 0.20 was simulated, respectively. The

simulated results of interaction energies and crystal habit properties are summarized in Table 5. The negative interaction energies of  $\epsilon$ -HNIW crystal/solvent systems indicate that the adsorption of solvent molecules on  $\epsilon$ -HNIW faces is exothermic and thermodynamically favourable [5]. The predicted morphologies of  $\epsilon$ -HNIW crystals affected by acetone–cyclohexane with different cyclohexane ratios are displayed in Fig. 6. In order to examine the accuracy of the simulation results,  $\epsilon$ -HNIW crystals were cultivated in acetone–cyclohexane binary systems with cyclohexane mass fraction of 0.05, 0.10, 0.15 and 0.20

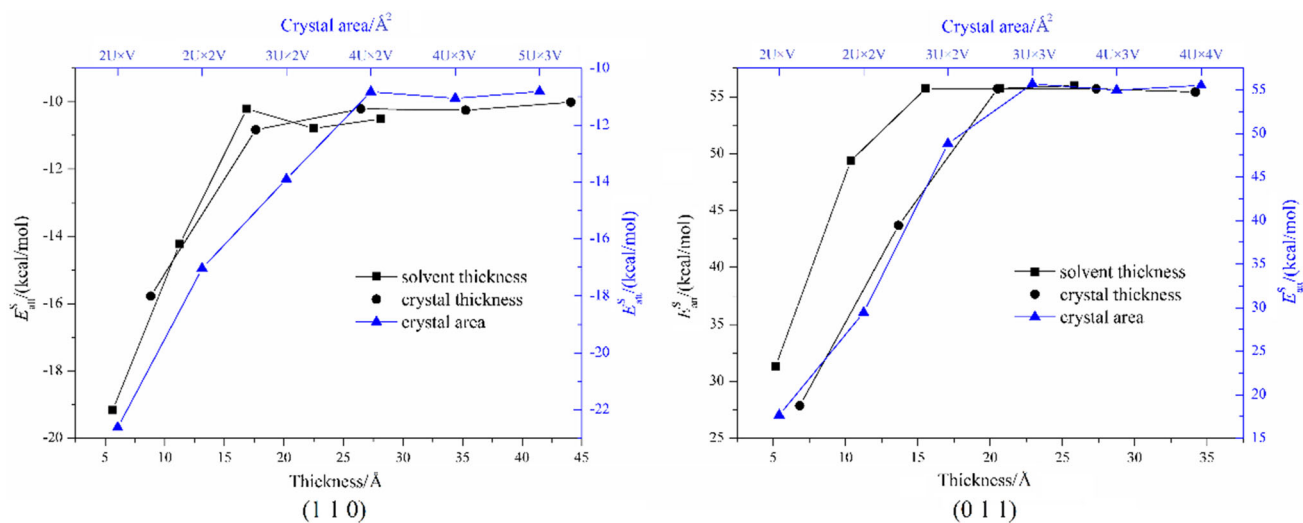


**Figure 4** Influence of model size on the  $E_{att}^S$ .

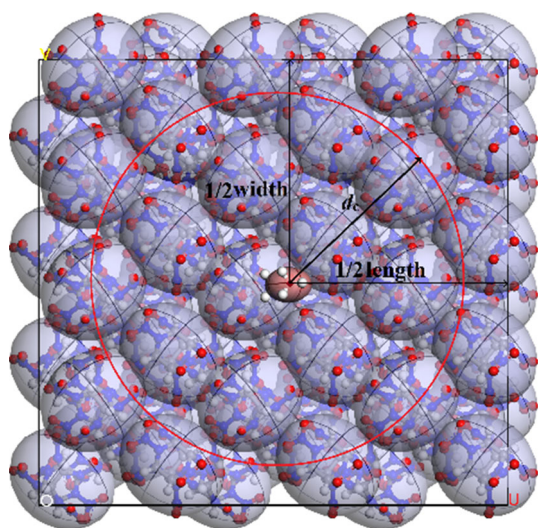


**Figure 5** Range of interaction between solvent and  $\epsilon$ -HNIW crystal.

at 298 K using incubator. As the mass fraction of anti-solvent has few influences on HNIW morphology, Fig. 6 only displays the SEM of  $\epsilon$ -HNIW in the acetone–cyclohexane binary system with the cyclohexane ratio of 0.2.

From the simulation results, it can be seen that only (1 1 0) and (1 1  $-$  1) are still exposed on  $\epsilon$ -HNIW crystals affected by solvents, probably because these two faces grow slower than others in acetone–cyclohexane binary systems. All the simulated crystal habits of  $\epsilon$ -HNIW present fusiform shape, which have a great agreement with the experimental results. Combining the computational and experimental results, it can be concluded that the simulation

method and the model size are suitable for the morphology study of  $\epsilon$ -HNIW. With the increase in anti-solvent ratio,  $\epsilon$ -HNIW crystal morphology almost maintains constant, and the aspect ratio, relative surface/volume ratio and the percentage area ( $S\%$ ) of  $\epsilon$ -HNIW-exposed crystal faces change little as well. So, it is impossible to control  $\epsilon$ -HNIW crystal morphology by changing cyclohexane ratio. Assuming that the increase in cyclohexane is a continuous process, this simulation can be regarded as the anti-solvent crystallization process. Assuming that  $\epsilon$ -HNIW crystal nuclei start to generate when the mass fraction of cyclohexane reaches 0.05 and  $\epsilon$ -HNIW crystals continue to grow with the increase in cyclohexane ratio from 0.05 to 0.20, it can be demonstrated that the morphology of crystal is mainly determined by the nucleation step in the crystallization process through the simulation. When the nucleation is occurred, the morphology will stay unchanged without the addition of other additives.

### The influence of different anti-solvents on $\epsilon$ -HNIW morphology

The difference in polarity and dipole moment between different anti-solvents may result in different interactions between anti-solvent molecules and crystals, thus having a large influence on crystal morphology. Based on this, the influences of acetone–cyclohexane, acetone–toluene, acetone–benzene and acetone–dichloromethane on  $\epsilon$ -HNIW crystal morphology were investigated to figure out whether



**Table 5** Interaction energies and modified attachment energies of  $\epsilon$ -HNIW crystal faces in acetone–cyclohexane binary systems with different cyclohexane mass fractions

Ratio	$E$ (kcal mol <sup>-1</sup> )	(1 1 0)	(1 1 - 1)	(0 0 1)	(2 0 0)	(0 1 1)	(2 0 - 1)
0.05	$E_{tot}$	- 21557.18	- 35672.10	- 24337.21	- 24102.69	- 35947.31	- 23988.63
	$E_{sur}$	- 18614.70	- 31724.81	- 20778.86	- 21119.91	- 31412.24	- 20975.50
	$E_{sol}$	- 2560.54	- 3386.01	- 2979.70	- 2613.00	- 3824.51	- 2505.40
	$E_{int}$	- 381.94	- 561.28	- 578.65	- 369.79	- 710.56	- 507.72
	$E_S$	- 76.10	- 85.11	- 111.62	- 39.54	- 155.49	- 127.43
	$E_{att}^S$	- 10.61	- 7.86	21.91	- 55.36	57.55	15.13
	S%	41.16	58.84	0.00	0.00	0.00	0.00
	Aspect ratio		2.64	Relative surface/volume ratio			1.236
0.10	$E_{tot}$	- 21250.97	- 35517.18	- 24185.52	- 24035.09	- 35536.43	- 23883.48
	$E_{sur}$	- 18620.89	- 26031.03	- 17187.74	- 21208.95	- 31398.64	- 20964.76
	$E_{sol}$	- 2250.14	- 8926.39	- 6416.24	- 2458.91	- 3425.03	- 2409.65
	$E_{int}$	- 379.95	- 559.75	- 581.54	- 367.23	- 712.75	- 509.07
	$E_S$	- 75.70	- 84.87	- 112.18	- 39.27	- 155.97	- 127.77
	$E_{att}^S$	- 11.01	- 8.09	22.47	- 55.64	58.03	15.47
	S%	40.81	59.19	0.00	0.00	0.00	0.00
	Aspect ratio		2.66	Relative surface/volume ratio			1.238
0.15	$E_{tot}$	- 21244.94	- 35406.72	- 23993.93	- 23764.97	- 35313.69	- 23627.15
	$E_{sur}$	- 18627.61	- 31721.86	- 20796.73	- 21147.31	- 31405.15	- 20955.94
	$E_{sol}$	- 2231.44	- 3119.20	- 2613.69	- 2243.48	- 3206.14	- 2162.44
	$E_{int}$	- 385.89	- 565.66	- 583.51	- 374.18	- 702.40	- 508.77
	$E_S$	- 76.89	- 85.77	- 112.56	- 40.01	- 153.71	- 127.70
	$E_{att}^S$	- 9.82	- 7.20	22.85	- 54.89	55.76	15.40
	S%	40.65	59.35	0.00	0.00	0.00	0.00
	Aspect ratio		2.66	Relative surface/volume ratio			1.238
0.20	$E_{tot}$	- 21282.51	- 35353.53	- 23923.70	- 23693.17	- 35167.34	- 24734.75
	$E_{sur}$	- 18640.64	- 31682.03	- 20791.65	- 21194.90	- 31427.61	- 20954.88
	$E_{sol}$	- 2261.02	- 3108.09	- 2554.81	- 2136.54	- 3037.61	- 3274.45
	$E_{int}$	- 380.84	- 563.41	- 577.24	- 361.73	- 702.13	- 505.42
	$E_S$	- 75.88	- 85.43	- 111.35	- 38.68	- 153.65	- 126.86
	$E_{att}^S$	- 10.83	- 7.54	21.64	- 56.22	55.70	14.55
	S%	38.41	61.59	0.00	0.00	0.00	0.00
	Aspect ratio		2.76	Relative surface/volume ratio			1.248

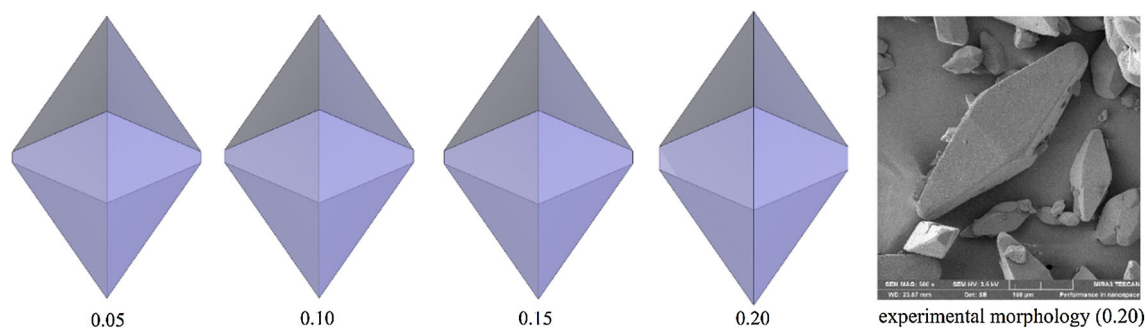


**Figure 6** Morphology of  $\epsilon$ -HNIW crystals in acetone–cyclohexane binary systems with different cyclohexane mass fractions.

different anti-solvents can affect  $\epsilon$ -HNIW crystal morphology differently. The simulated results of

interaction energies and crystal habit properties are summarized in Table 6, and the predicted

**Table 6** Interaction energies and modified attachment energies of  $\epsilon$ -HNIW crystal faces in different binary systems

Solvent	$E$ (kcal mol <sup>-1</sup> )	(1 1 0)	(1 1 - 1)	(0 0 1)	(2 0 0)	(0 1 1)	(2 0 - 1)
C <sub>3</sub> H <sub>6</sub> O/C <sub>6</sub> H <sub>12</sub>	$E_{\text{tot}}$	- 21282.51	- 35353.53	- 23923.70	- 23693.17	- 35167.34	- 24734.75
	$E_{\text{sur}}$	- 18640.64	- 31682.03	- 20791.65	- 21194.90	- 31427.61	- 20954.88
	$E_{\text{sol}}$	- 2261.02	- 3108.09	- 2554.81	- 2136.54	- 3037.61	- 3274.45
	$E_{\text{int}}$	- 380.84	- 563.41	- 577.24	- 361.73	- 702.13	- 505.42
	$E_{\text{S}}$	- 75.88	- 85.43	- 111.35	- 38.68	- 153.65	- 126.86
	$E_{\text{att}}^{\text{S}}$	- 10.83	- 7.54	21.64	- 56.22	55.70	14.55
	S%	38.41	61.59	0.00	0.00	0.00	0.00
	Aspect ratio		2.76	Relative surface/volume ratio			1.248
C <sub>3</sub> H <sub>6</sub> O/C <sub>7</sub> H <sub>8</sub>	$E_{\text{tot}}$	- 20960.25	- 34947.15	- 23609.49	- 16213.41	- 34845.31	- 23313.09
	$E_{\text{sur}}$	- 14464.43	- 31696.97	- 20813.08	- 13879.81	- 31438.77	- 20935.34
	$E_{\text{sol}}$	- 6097.44	- 2672.35	- 2240.12	- 1954.63	- 2686.61	- 1904.84
	$E_{\text{int}}$	- 398.37	- 577.84	- 556.29	- 378.97	- 719.94	- 472.91
	$E_{\text{S}}$	- 79.38	- 87.62	- 107.31	- 40.52	- 157.54	- 118.70
	$E_{\text{att}}^{\text{S}}$	- 7.34	- 5.35	17.60	- 54.38	59.60	6.40
	S%	36.45	54.90	0.00	0.00	0.00	8.64
	Aspect ratio		2.67	Relative surface/volume ratio			1.216
C <sub>3</sub> H <sub>6</sub> O/C <sub>6</sub> H <sub>6</sub>	$E_{\text{tot}}$	- 21783.29	- 34973.85	- 24014.57	- 24244.25	- 34718.17	- 24186.99
	$E_{\text{sur}}$	- 18632.39	- 31690.20	- 20763.33	- 21138.31	- 31386.47	- 20934.44
	$E_{\text{sol}}$	- 2736.94	- 2690.40	- 2674.92	- 2746.72	- 2607.49	- 2757.45
	$E_{\text{int}}$	- 413.96	- 593.25	- 576.32	- 359.23	- 724.21	- 495.10
	$E_{\text{S}}$	- 82.48	- 89.95	- 111.17	- 38.41	- 158.48	- 124.27
	$E_{\text{att}}^{\text{S}}$	- 4.23	- 3.01	21.46	- 56.49	60.54	11.96
	S%	62.74	37.26	0.00	0.00	0.00	0.00
	Aspect ratio		2.42	Relative surface/volume ratio			1.220
C <sub>3</sub> H <sub>6</sub> O/CH <sub>2</sub> Cl <sub>2</sub>	$E_{\text{tot}}$	- 22227.48	- 35345.26	- 23724.89	- 24737.66	- 35004.64	- 24630.99
	$E_{\text{sur}}$	- 18655.81	- 31680.61	- 20766.11	- 21119.53	- 31368.73	- 20955.07
	$E_{\text{sol}}$	- 3153.18	- 3071.28	- 2392.63	- 3244.39	- 2912.69	- 3170.82
	$E_{\text{int}}$	- 418.48	- 593.38	- 566.14	- 373.74	- 723.22	- 505.11
	$E_{\text{S}}$	- 83.38	- 89.97	- 109.21	- 39.96	- 158.26	- 126.78
	$E_{\text{att}}^{\text{S}}$	- 3.33	- 2.99	19.50	- 54.94	60.32	14.48
	S%	50.27	49.73	0.00	0.00	0.00	0.00
	Aspect ratio		2.33	Relative surface/volume ratio			1.213

morphology of  $\epsilon$ -HNIW crystals affected by different binary systems is displayed in Fig. 7. The morphologies of  $\epsilon$ -HNIW crystal, cultivating from acetone–cyclohexane, acetone–toluene, acetone–benzene and acetone–dichloromethane at 298 K, are depicted in Fig. 7 as well.

The simulation results show that all the  $\epsilon$ -HNIW crystals grown from these four systems assume fusiform shape, though there are differences in aspect ratio, relative surface/volume ratio and S% between each other. Besides, there are three dominant faces exposed on  $\epsilon$ -HNIW crystals in acetone–toluene system, while there are only two in other cases, because the interaction energy between the (2 0 - 1) face and solvent molecules is much higher in acetone–toluene system than those in other systems, which makes it

more difficult to remove the acetone–toluene molecules attached on the surface. Therefore, the growth rate of the (2 0 - 1) face in acetone–toluene is slower than those in other systems, which results in (2 0 - 1) exposed on  $\epsilon$ -HNIW crystal surface. The  $\epsilon$ -HNIW crystal was cultivated in acetone–cyclohexane, acetone–toluene, acetone–benzene and acetone–dichloromethane at 298 K, respectively. The experimental morphology of  $\epsilon$ -HNIW shows a great agreement with the simulation results, which demonstrated that the computation can provide guidances for the experiment. The simulation and experiment results reveal that anti-solvents can significantly affect the growth rate of (2 0 - 1) face that influences the crystal morphology. And the acetone–toluene binary solution contributes to the preparation of spherical

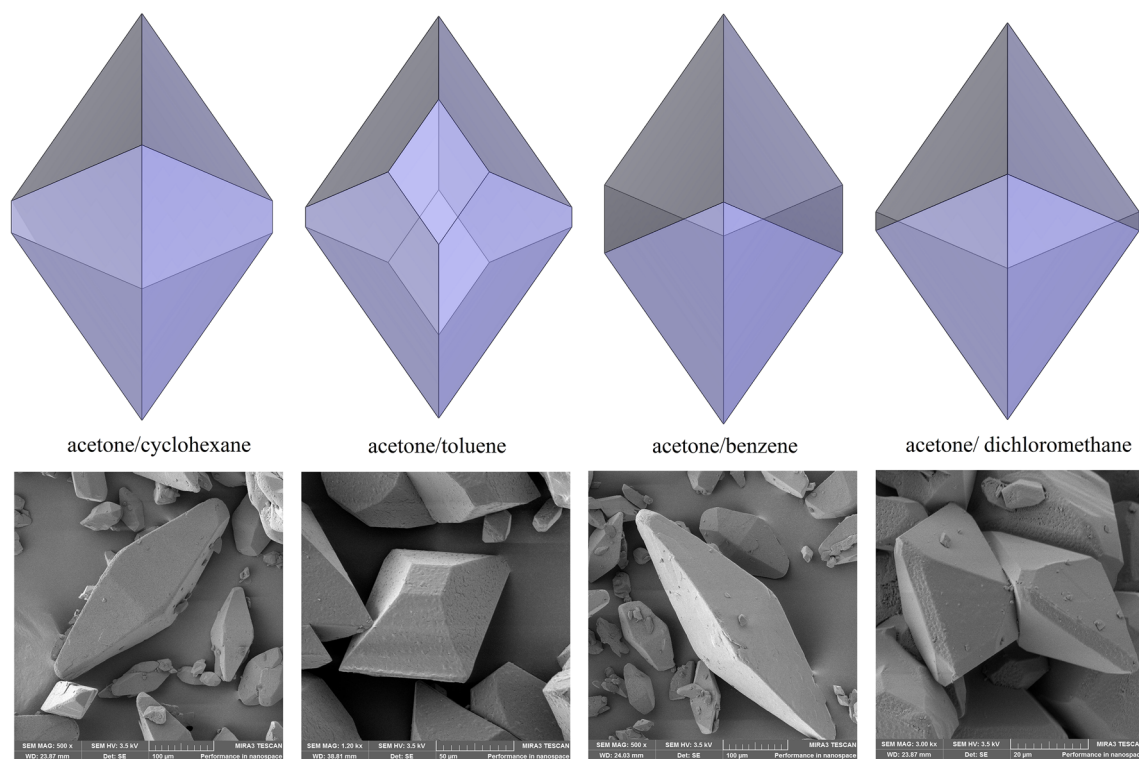


**Figure 7** Morphology of  $\epsilon$ -HNIW crystals in different binary systems.

crystals of  $\epsilon$ -HNIW than acetone–cyclohexane, acetone–benzene and acetone–dichloromethane.

### The influence of temperature on $\epsilon$ -HNIW crystal morphology

Temperature greatly affects the growth rate, nucleation rate, solubility, supersaturation and hence the morphology of crystals [6, 31]. Accordingly, the attachment energies at different temperatures were calculated to explore the relationship between  $\epsilon$ -HNIW crystal morphology and temperature. The simulated results are summarized in Table 7, and the predicted morphology of  $\epsilon$ -HNIW crystals at different temperature is displayed in Fig. 8. The morphologies of  $\epsilon$ -HNIW crystal, cultivating from acetone–cyclohexane at 298, 308, 318 and 328 K, are depicted in Fig. 8 as well.

Comparing the morphology of  $\epsilon$ -HNIW crystals predicted at different temperatures, it can be concluded that the areas of the (0 0 1) (2 0 – 1) faces increase with the increase in temperature. It is because higher temperature makes the attachment energy between (0 0 1) or (2 0 – 1) and solvent molecules decrease, causing these two faces to grow

slower and appear in the final  $\epsilon$ -HNIW crystal surface. The simulated results show a great agreement with the experimental outcomes. The experimental results show that with the increase in temperature the particle diameter of  $\epsilon$ -HNIW presents the tendency of decrease. The simulation and experiment results reveal that temperature can significantly affect the growth rate of (2 0 – 1) face that influences the crystal morphology. Combining the computational and experimental results, it can be concluded that the increasing temperature makes the aspect ratio decrease and the number of surface increase, which indicates that higher temperature contributes to the preparation of spherical crystals of  $\epsilon$ -HNIW.

### The influence of supersaturation on $\epsilon$ -HNIW crystal morphology

Supersaturation greatly affects the rate of growth, nucleation rate and hence the morphology of the crystals [22, 31]. Generally, higher supersaturation contributes to nucleation and makes the final crystal volume small. Accordingly, a double-layered model (Fig. 9) was built for the calculation of the attachment energies in acetone–cyclohexane (0.2) with different

**Table 7** Interaction energies and modified attachment energies of  $\epsilon$ -HNIW crystal faces in acetone–cyclohexane (0.2) binary systems at different temperatures

$T$ (K)	$E$ (kcal mol <sup>-1</sup> )	(1 1 0)	(1 1 - 1)	(0 0 1)	(2 0 0)	(0 1 1)	(2 0 - 1)
298	$E_{\text{tot}}$	- 21282.51	- 35353.53	- 23923.70	- 23693.17	- 35167.34	- 24734.75
	$E_{\text{sur}}$	- 18640.64	- 31682.03	- 20791.65	- 21194.90	- 31427.61	- 20954.88
	$E_{\text{sol}}$	- 2261.02	- 3108.09	- 2554.81	- 2136.54	- 3037.61	- 3274.45
	$E_{\text{int}}$	- 380.84	- 563.41	- 577.24	- 361.73	- 702.13	- 505.42
	$E_{\text{S}}$	- 75.88	- 85.43	- 111.35	- 38.68	- 153.65	- 126.86
	$E_{\text{att}}^{\text{S}}$	- 10.83	- 7.54	21.64	- 56.22	55.70	14.55
	S%	38.41	61.59	0.00	0.00	0.00	0.00
	Aspect ratio		2.76	Relative surface/volume ratio			1.248
308	$E_{\text{tot}}$	- 21465.88	- 35028.15	- 23765.84	- 23474.22	- 34928.56	- 23108.41
	$E_{\text{sur}}$	- 18537.45	- 31546.28	- 20699.54	- 20998.52	- 31273.60	- 20702.98
	$E_{\text{sol}}$	- 2543.08	- 2927.27	- 2497.59	- 2116.89	- 2962.77	- 1907.60
	$E_{\text{int}}$	- 385.35	- 554.60	- 568.71	- 358.82	- 692.19	- 497.84
	$E_{\text{S}}$	- 76.78	- 84.09	- 109.70	- 38.37	- 151.47	- 124.95
	$E_{\text{att}}^{\text{S}}$	- 9.93	- 8.87	20.00	- 56.54	53.53	12.65
	S%	49.31	48.98	0.00	0.00	0.00	1.71
	Aspect ratio		2.34	Relative surface/volume ratio			1.21
318	$E_{\text{tot}}$	- 20860.92	- 34863.53	- 23626.20	- 23359.74	- 34657.95	- 23332.01
	$E_{\text{sur}}$	- 18475.39	- 31489.72	- 20639.29	- 20975.67	- 31122.50	- 20842.46
	$E_{\text{sol}}$	- 1997.45	- 2823.29	- 2423.81	- 2030.19	- 2828.84	- 1996.28
	$E_{\text{int}}$	- 388.07	- 550.52	- 563.10	- 353.89	- 706.61	- 493.27
	$E_{\text{S}}$	- 77.32	- 83.47	- 108.62	- 37.84	- 154.63	- 123.81
	$E_{\text{att}}^{\text{S}}$	- 9.39	- 9.49	18.91	- 57.06	56.69	11.50
	S%	53.72	42.14	0.07	0.00	0.00	4.07
	Aspect ratio		2.14	Relative surface/volume ratio			1.19
328	$E_{\text{tot}}$	- 20739.78	- 34566.55	- 23426.34	- 23199.77	- 34547.36	- 23093.83
	$E_{\text{sur}}$	- 18401.99	- 31334.26	- 20505.61	- 20883.70	- 31014.36	- 20711.00
	$E_{\text{sol}}$	- 1947.45	- 2687.23	- 2363.25	- 1966.44	- 2835.64	- 1893.69
	$E_{\text{int}}$	- 390.34	- 545.07	- 557.48	- 349.63	- 697.37	- 489.13
	$E_{\text{S}}$	- 77.78	- 82.65	- 107.53	- 37.38	- 152.61	- 122.77
	$E_{\text{att}}^{\text{S}}$	- 8.94	- 10.32	17.83	- 57.52	54.66	10.47
	S%	57.48	33.91	0.74	0.00	0.00	7.87
	Aspect ratio		2.12	Relative surface/volume ratio			1.18

supersaturations to explore the relationship between  $\epsilon$ -HNIW crystal morphology and supersaturation. The simulated results are summarized in Table 8, and the predicted morphology of  $\epsilon$ -HNIW crystals affected by acetone–cyclohexane systems with different supersaturations is displayed in Fig. 10.

The increasing supersaturation can hardly change the aspect ratios and relative surface/volume ratios of  $\epsilon$ -HNIW crystals. However, the volumes decrease and the areas of (0 0 1) (2 0 - 1) increase evidently with the increase in supersaturation. The nucleation competes with the crystal growth in the crystallization process, based on which higher supersaturation

contributes to the nucleation and helps prepare crystals of small particle, while lower supersaturation is conducive to the crystal growth and the preparation of crystals of large particle. Higher supersaturation makes the nucleation possess a higher rate compared with the crystal growth, which is difficult for the growth of most crystal faces. As a result, only the (0 0 1) (2 0 - 1) are exposed on the final  $\epsilon$ -HNIW crystal surface.

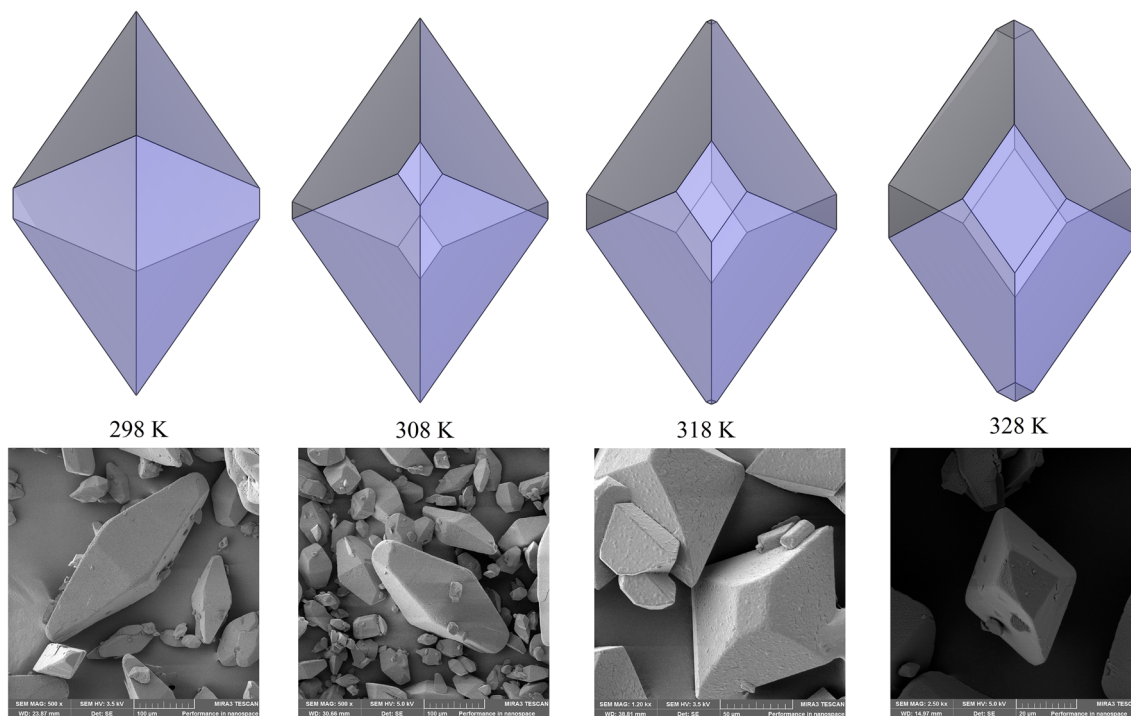
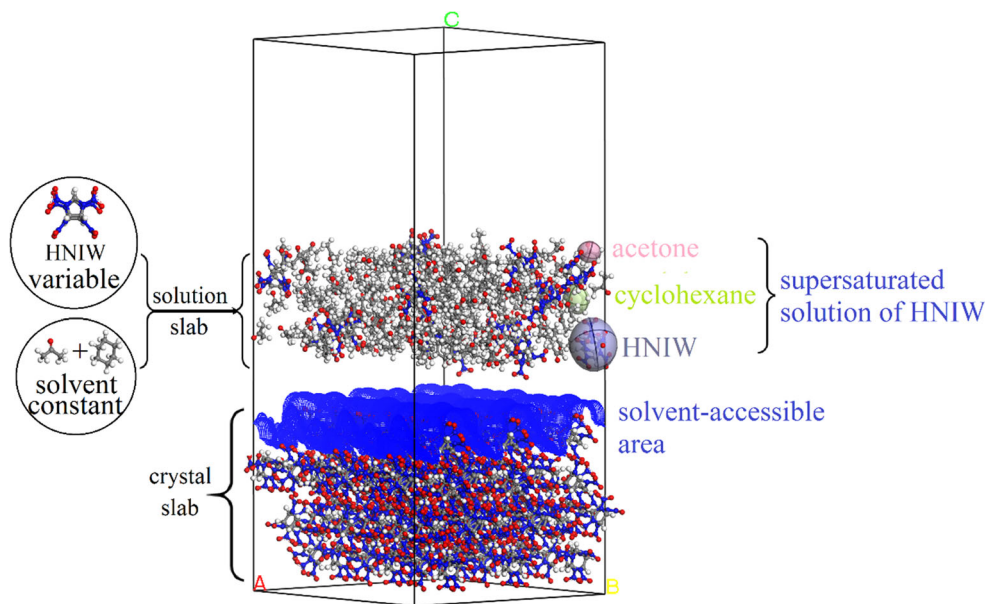


**Figure 8** Morphology of  $\epsilon$ -HNIW crystals in acetone–cyclohexane (0.2) binary systems at different temperatures.

**Figure 9** Double-layered model for attachment energy calculation.



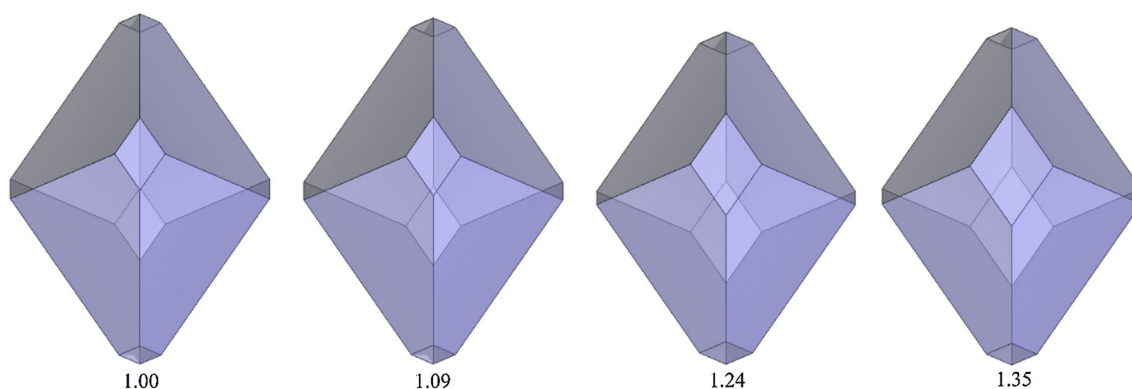
### Radial distribution function (RDF) of the interfacial model

In statistical mechanics, the RDF in a system of particles (atoms, molecules, colloids, etc.) describes how density varies as a function of distance from a reference particle. It is a measure of the probability of finding a particle at a distance of  $r$  away from a given

reference particle. The RDF analysis is widely used in structural investigations of both solid and liquid packings, studying specific interactions such as hydrogen bonds and van der Waals forces. Ordinarily, the distance ranges of hydrogen bonding interactions and van der Waals interactions are within 3.1 and 3.1–5.0 Å, respectively. In contrast, the electrostatic interactions exhibit a large distance range of

**Table 8** Interaction energies and modified attachment energies of  $\epsilon$ -HNIW crystal faces in acetone–cyclohexane (0.2) binary systems with different supersaturations

Supersaturation	$E$ (kcal mol <sup>-1</sup> )	(1 1 0)	(1 1 - 1)	(0 0 1)	(2 0 0)	(0 1 1)	(2 0 - 1)	
1.00	$E_{\text{tot}}$	- 23283.18	- 38651.07	- 26586.03	- 25706.45	- 38418.56	- 25661.47	
	$E_{\text{sur}}$	- 18641.43	- 31717.52	- 20724.31	- 21130.21	- 31391.95	- 20955.87	
	$E_{\text{sol}}$	- 4258.05	- 6381.65	- 5307.83	- 4219.39	- 6349.69	- 4206.84	
	$E_{\text{int}}$	- 383.70	- 551.90	- 553.89	- 356.85	- 676.93	- 498.76	
	$E_{\text{S}}$	- 76.45	- 83.68	- 106.84	- 38.16	- 148.13	- 125.18	
	$E_{\text{att}}^{\text{S}}$	- 10.26	- 9.28	17.14	- 56.75	50.19	12.88	
	S%	49.28	47.45	1.15	0.00	0.00	2.12	
	Aspect ratio	2.08	Relative surface/volume ratio		1.19	Volume		6.92
	1.09	$E_{\text{tot}}$	- 23828.43	- 39504.61	- 27154.92	- 26325.86	- 39335.01	- 26167.38
$E_{\text{sur}}$		- 18623.09	- 31653.01	- 20821.45	- 21119.53	- 31400.81	- 20936.56	
$E_{\text{sol}}$		- 4820.49	- 7296.15	- 5785.13	- 4846.90	- 7247.15	- 4735.83	
$E_{\text{int}}$		- 384.85	- 555.44	- 548.34	- 359.43	- 687.05	- 494.99	
$E_{\text{S}}$		- 76.68	- 84.22	- 105.77	- 38.43	- 150.35	- 124.24	
$E_{\text{att}}^{\text{S}}$		- 10.03	- 8.75	16.07	- 56.47	52.40	11.94	
S%		47.17	48.56	1.45	0.00	0.00	2.81	
Aspect ratio		2.10	Relative surface/volume ratio		1.19	Volume		6.11
1.24		$E_{\text{tot}}$	- 24151.95	- 39849.52	- 27777.57	- 26652.76	- 39635.62	- 26289.10
	$E_{\text{sur}}$	- 18624.19	- 31707.09	- 20802.41	- 21140.77	- 31442.50	- 20950.74	
	$E_{\text{sol}}$	- 5142.73	- 7586.38	- 6429.90	- 5150.52	- 7521.90	- 4846.89	
	$E_{\text{int}}$	- 385.02	- 556.05	- 545.25	- 361.48	- 671.22	- 491.47	
	$E_{\text{S}}$	- 76.71	- 84.31	- 105.18	- 38.65	- 146.88	- 123.36	
	$E_{\text{att}}^{\text{S}}$	- 10.00	- 8.65	15.47	- 56.25	48.94	11.05	
	S%	45.94	47.62	1.94	0.00	0.00	4.50	
	Aspect ratio	2.08	Relative surface/volume ratio		1.18	Volume		5.92
	1.35	$E_{\text{tot}}$	- 24710.97	- 38746.31	- 28433.45	- 27199.73	- 40442.96	- 26838.64
$E_{\text{sur}}$		- 18636.16	- 31711.87	- 20782.35	- 21113.20	- 31400.33	- 20960.61	
$E_{\text{sol}}$		- 5689.47	- 6478.89	- 7104.62	- 5726.00	- 8370.00	- 5389.01	
$E_{\text{int}}$		- 385.34	- 555.55	- 546.47	- 360.53	- 672.63	- 489.02	
$E_{\text{S}}$		- 76.78	- 84.24	- 105.41	- 38.55	- 147.19	- 122.74	
$E_{\text{att}}^{\text{S}}$		- 9.93	- 8.73	15.71	- 56.35	49.25	10.44	
S%		46.07	46.05	1.74	0.00	0.00	6.13	
Aspect ratio		2.08	Relative surface/volume ratio		1.19	Volume		5.87

**Figure 10** Morphology of  $\epsilon$ -HNIW crystals in acetone–cyclohexane (0.2) binary systems with different supersaturation.

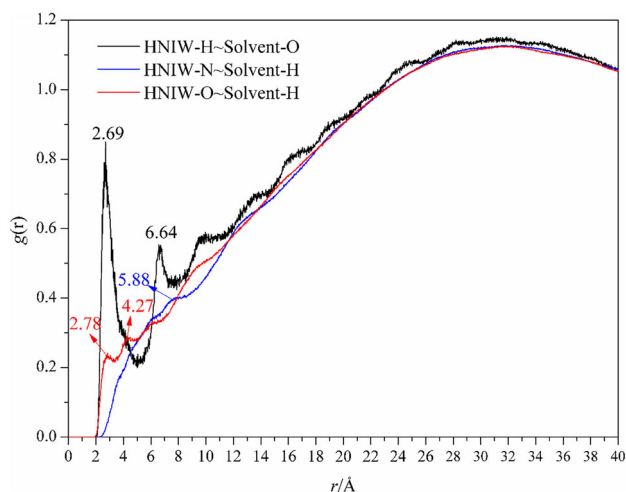


**Figure 11** Radial distribution function of the double-layered model of  $\epsilon$ -HNIW and the binary system.

above 5.0 Å [10]. Taking the (1 1 0) face and acetone-cyclohexane binary system with cyclohexane mass fraction of 0.20 for example, the RDF diagram of  $\epsilon$ -HNIW-O ~ solvent-H,  $\epsilon$ -HNIW-N ~ solvent-H and  $\epsilon$ -HNIW-H ~ solvent-O is displayed in Fig. 11.

In Fig. 11, there are two strong peaks on the RDF curve of  $\epsilon$ -HNIW-H ~ solvent-O, within 3.1 Å and above 5.0 Å, respectively, which illustrates that hydrogen bonding and electrostatic interaction may exist between  $\epsilon$ -HNIW-H and solvent-O. Moreover, the intensities of these two peaks are larger than  $\epsilon$ -HNIW-O ~ solvent-H and  $\epsilon$ -HNIW-N ~ solvent-H peaks, which indicates the interactions between  $\epsilon$ -HNIW surface and solvent molecules mainly consist of the interaction between  $\epsilon$ -HNIW-H and solvent-O. Similarly, there are two weak peaks on the RDF curve of  $\epsilon$ -HNIW-O ~ solvent-H, within 3.1 and 3.1–5.0 Å, respectively, which illustrates that hydrogen bonds and van der Waals forces may exist between  $\epsilon$ -HNIW-O and solvent-H. There is no obvious peak on the RDF curve of  $\epsilon$ -HNIW-N ~ solvent-H, illustrating that the interaction between  $\epsilon$ -HNIW-N and solvent-H is weak. Since the binding energy of hydrogen bonding is higher than Van der Waals forces and Coulomb interaction, for the same surface, the existence of hydrogen bonding will consume more energy for the growth of  $\epsilon$ -HNIW, and thus, the surface area of the crystal will be large. On the contrary, if there is not hydrogen bonding, the surface area will be small. Therefore, we can select a solvent which can form hydrogen bonding with the surface of large area and not form hydrogen bonding with

the surface of small area to ameliorate crystal morphology.

## Conclusions

The morphology and dominant faces of  $\epsilon$ -HNIW crystals in vacuum and binary systems were predicted by the AE model. Then, the RDF was employed to analyse the interaction energies between  $\epsilon$ -HNIW surface and solvent molecules. The major results obtained can be summarized as follows:

1. The size of  $\epsilon$ -HNIW/binary system interfacial model used for molecular dynamic simulations was modified, of which the length, width and thickness of the  $\epsilon$ -HNIW supercell should be larger than  $2d_c$ ,  $2d_c$  and  $d_c$ , respectively, and the thickness of solvent amorphous cell should be larger than  $d_c$ .
2. Some morphological important faces of  $\epsilon$ -HNIW crystals disappear with the effect of solvent molecules. Therefore, external growth environments have great influence on  $\epsilon$ -HNIW crystal morphology, which can help prepare products of specific shape to meet the requirements of different applications.
3. The RDF analysis demonstrates that the interaction energies between  $\epsilon$ -HNIW and solvents that cause the variation of the attachment energies may consist of hydrogen bonds and electrostatic interactions between  $\epsilon$ -HNIW-H and solvent-O. By comparison, the interactions between  $\epsilon$ -HNIW-O,  $\epsilon$ -HNIW-N and solvent-H are relatively weak.

## Acknowledgements

The work was supported by the Fundamental Research Funds for the Central Universities.

## References

- [1] Nielsen AT (1997) Caged polynitramine compound. US Pat 5,693,794
- [2] Lobbecke S, Bohn MA, Pfeil A (1998) Thermal behavior and stability of HNIW (CL-20). In: Proceedings of 29th international conference of ICT, Karlsruhe

- [3] Vávra P (1999) Procedure for selection of molecular structures of explosives having high performance. In: Proceedings of 30th international conference of ICT, Karlsruhe
- [4] Zhou Q, Chen Z, Zheng C, Wang B, Ren X, Wang K, Wang M, Zhou C (2014) Effect of morphology of FOX-7 crystals on its sensitivity. *Chin J Explos Propellants* 37:67–69
- [5] Shi W, Xia M, Lei W, Wang F (2014) Solvent effect on the crystal morphology of 2,6-diamino-3,5-dinitropyridine-1-oxide: a molecular dynamics simulation study. *J Mol Graph Model* 50:71–77
- [6] Singh MK, Banerjee A (2013) Role of solvent and external growth environments to determine growth morphology of molecular crystals. *Cryst Growth Des* 6:2413–2425
- [7] Hod I, Mastai Y, Medina DD (2011) Effect of solvents on the growth morphology of DL-alanine crystals. *Cryst Eng Commun* 2:502–509
- [8] Li C, Choi P (2008) Molecular dynamics study on the effect of solvent adsorption on the morphology of glycothermally produced  $\alpha$ -Al<sub>2</sub>O<sub>3</sub> particles. *J Phys Chem C* 112:10145–10152
- [9] Hors JH, Geertman RM, Rosmalen GM (2001) The effect of solvent on crystal morphology. *J Cryst Growth* 230:277–284
- [10] Liu N, Li Y, Zeman S, Shu Y, Wang B, Zhou Y, Zhao Q, Wang W (2016) Crystal morphology of 3,4-bis(3-nitrofuran-4-yl)furoxan (DNTF) in a solvent system: molecular dynamics simulation and sensitivity study. *CrystEngComm* 18:2843–2851
- [11] Feng L, Cao D, Wang J, Chen L, Chen F, Zhang N, Liu P (2015) Prediction of crystal morphology of MTIN. *Chin J Energy Mater* 23:443–449
- [12] Xiong S, Chen S, Jin S, Li L (2016) Additives effects on crystal morphology of dihydroxylammonium 5,5'-Bistetrazole-1,1'-diolate by molecular dynamics simulations. *J Energy Mater* 34:384–394
- [13] Wang D, Chen S, Li Y, Yang J, Wei T, Li L (2015) Effect of solvent on the crystal morphology of royal demolition explosive. *J Beijing Inst Technol* 24:260–268
- [14] Yan T, Wang J, Liu Y, Zhao J, Yuan J, Guo J (2015) Growth and morphology of 1,3,5,7-tetranitro-1,3,5,7-tetraazacyclooctane (HMX) crystal. *J Cryst Growth* 430:7–13
- [15] Chen G, Xia M, Lei W, Wang F, Gong X (2013) A study of the solvent effect on the morphology of RDX crystal by molecular modeling method. *J Mol Model* 19:5397–5406
- [16] Berkovitch-Yellin Z (1985) Toward an ab initio derivation of crystal morphology. *J Am Chem Soc* 107:8239–8253
- [17] Jin SH, Lei XD, Ou YX, Liu JQ, Song QC (2005) Influence of anti-solvent property on the modes of crystallization of HNIW. *Acta Armamentarii* 26:743–745
- [18] Xiong SL, Chen SS, Jin SH, Li LJ (2016) Additives effects on crystal morphology of dihydroxylammonium 5,5'-bistetrazole-1,1'-diolate by molecular dynamics simulations. *J Energy Mater* 4:384–394
- [19] Mao XL, Song XF, Lu GM, Xu YX, Sun YZ, Yu JG (2015) Effect of additives on the morphology of calcium sulfate hemihydrate: experimental and molecular dynamics simulation studies. *Chem Eng J* 278:320–327
- [20] Chen F, Liu YY, Wang JL, Su NN, Li LJ, Chen HC (2017) Investigation of the co-solvent effect on the crystal morphology of  $\beta$ -HMX using molecular dynamics simulations. *Acta Phys Chim Sin* 33:1140–1148
- [21] Chen G, Chen CY, Xia MZ, Lei W, Wang FY, Gong XD (2015) Molecular dynamics investigation of the effect of solvent adsorption on crystal habits of hexogen. *RSC Adv* 5:25581–25589
- [22] Wang C, Zhang X, Du W, Huang YH, Guo MX, Li Y, Zhang ZX, Hou BH, Yin QX (2016) Effects of solvent and supersaturation on crystal morphology of cefaclor dihydrate: a combined experimental and computer simulation study. *CrystEngComm* 18:9085–9094
- [23] Chen G, Xia MZ, Lei W, Wang FY, Gong XD (2014) Molecular dynamics investigation of the effect of solvent adsorption on crystal habits of hexogen. *Can J Chem* 92:849–854
- [24] Leamy HJ, Gilmer GH, Jackson KA, Blakely JM (1975) Surface physics of materials. Academic Press, New York
- [25] Kim JW, Park DB, Shim HM, Kim HS, Koo KK (2012) Crystallization of RDX by drowning-out combined with fines dissolution and cooling process. *Ind Eng Chem Res* 51:3758–3765
- [26] Hartman P, Bennema P (1980) The attachment energy as a habit controlling factor: I. Theoretical considerations. *J Cryst Growth* 49:145–156
- [27] Zhang Y (2004) Ph.D. thesis, Tianjing university
- [28] Saska M, Myerson AS (1983) The theoretical shape of sucrose crystals from energy calculations. *J Cryst Growth* 61:546–555
- [29] Zhao X, Shi N (1996) Crystal and molecular structure of  $\epsilon$ -HNIW. *Chin Sci Bull* 41:574–576
- [30] Zhao Q, Liu N, Wang B, Wang W (2016) A study of solvent selectivity on the crystal morphology of FOX-7 via a modified attachment energy model. *RSC Adv* 6:59784–59793
- [31] Singh MK, Tiwari VS (2015) Uncovering the mode of action of solvent and additive controlled crystallization of urea crystal: a molecular-scale study. *Cryst Growth Des* 15:3220–3234